Origin of metal-insulator transition in rare-earth Nickelates

Swagata Acharya, ^{1,*} Brooks Tellekamp, ¹ Jerome Jackson, ² Dimitar Pashov, ³ Jeffrey L. Blackburn, ¹ Kirstin Alberi, ¹ and Mark van Schilfgaarde ¹

¹National Renewable Energy Laboratory, Golden, Colorado 80401 ²Scientific Computing Department, STFC Daresbury Laboratory, Warrington WA4 4AD, United Kingdom ³King's College London, Theory and Simulation of Condensed Matter, The Strand, WC2R 2LS London, UK

Rare-earth nickelates RNiO₃ (R=rare-earth element) exhibit three kinds of phase transitions with decreasing temperature: a structural transition from a pseudo-cubic to a monoclinic phase, a metal-insulator transition (MIT), and a magnetic transition from a paramagnetic state to an ordered one. The first two occur at the same temperature, which has led to a consensus that the MIT is driven by lattice distortions. We show here that the primary driving force for the MIT is magnetic; however because of the unusual d^7 configuration of Ni, additional flexibility in spin configurations are also needed which symmetry-lowing structural deformations make possible. The latter enable Ni to disproportionate into two kinds: a high-spin and a low-spin configuration, which allow the system to reduce its unfavorable orbital moment and also open a gap.

I. INTRODUCTION

Rare-earth nickelates RNiO₃ (R = rare-earth element) belong to the ABO₃ perovskite family and exhibit a rich phase diagram encompassing metal-insulator transitions (MIT), magnetic ordering, structural distortions, and even superconductivity under specific perturbations such as strain or doping. As the ionic radius of the rare-earth element increases (moving leftward across the lanthanide series), the critical temperature for the MIT decreases, with LuNiO₃ exhibiting the highest [1] and PrNiO₃ the lowest transition temperatures [2]. LaNiO₃ is a notable exception—it remains metallic down to the lowest measured temperatures and does not undergo any structural distortion [3]. The origin of the MIT has been a subject of intense debate, with two primary schools of thought: one attributing the transition to structural distortions, and the other to electronic and magnetic instabilities.

At high temperatures $(T > T_{\rm MIT})$, all RNiO₃ compounds (except LaNiO₃) adopt an orthorhombic *Pbnm* structure and exhibit a paramagnetic metallic phase. The degree of distortion from the ideal cubic perovskite structure in the *Pbnm* is influenced by the size of the rare-earth ion, which affects the Ni–O–Ni bond angle [4]. The larger the pseudo cubic distortion is, the higher $T_{\rm MIT}$ (Fig. 1). However, this structural tuning alone cannot explain the MIT. It is accompanied by a symmetry-lowering transition from the orthorhombic *Pbnm* to the monoclinic $P2_1/n$ phase. This transition entails a breathing-mode distortion, where NiO₆ octahedra alternate between expanded and contracted forms, leading to two inequivalent Ni sites [5, 6]. First-principles calculations have shown that this breathing mode is structurally triggered by oxygen octahedral rotations, and its softening is essential for the MIT [5]. The structural distortion thus appears necessary to stabilize the insulating phase.

However, several studies argue that the MIT is fundamentally electronic or magnetic in origin. Lau and Millis [7] proposed that the transition is driven by magnetism, with structural distortions playing a secondary, enabling role. Similarly, Badrtdinov et al. [6] demonstrated that the breathing-mode distortion is strongly coupled to the antiferromagnetic order, and that the competition between nearest-neighbor ferromagnetic and next-nearest-neighbor antiferromagnetic interactions determines the magnetic ground state. Further support for the electronic origin comes from hybrid functional and DFT+U+V calculations, which show that both on-site (U) and inter-site (V) Coulomb interactions are required to reproduce the insulating state and the observed bond disproportionation [8]. Without these electronic interactions, the breathing distortion and the band gap fail to emerge in simulations.

The unique magnetic nature of Ni cannot be overlooked either. Unlike its natural valence of 2^+ , Ni in these compounds nominally adopts a 3^+ valence state, corresponding to a partially filled magnetic d^7 configuration [9]. This configuration allows for multiple spin states and strong hybridization with oxygen ligands, leading to complex magnetic behavior. The structural transition from Pbnm to $P2_1/n$ typically takes the system from a paramagnetic metal to a paramagnetic insulator. Only for larger rare-earth radii (e.g., Nd, Pr) does the MIT coincide with a transition to an antiferromagnetic insulating phase [8]. Regardless of the rare-earth ion, magnetism, whether ordered or disordered, is omnipresent in both metallic and insulating phases. This raises a fundamental question: what role

^{*} swagata.acharya@nrel.gov

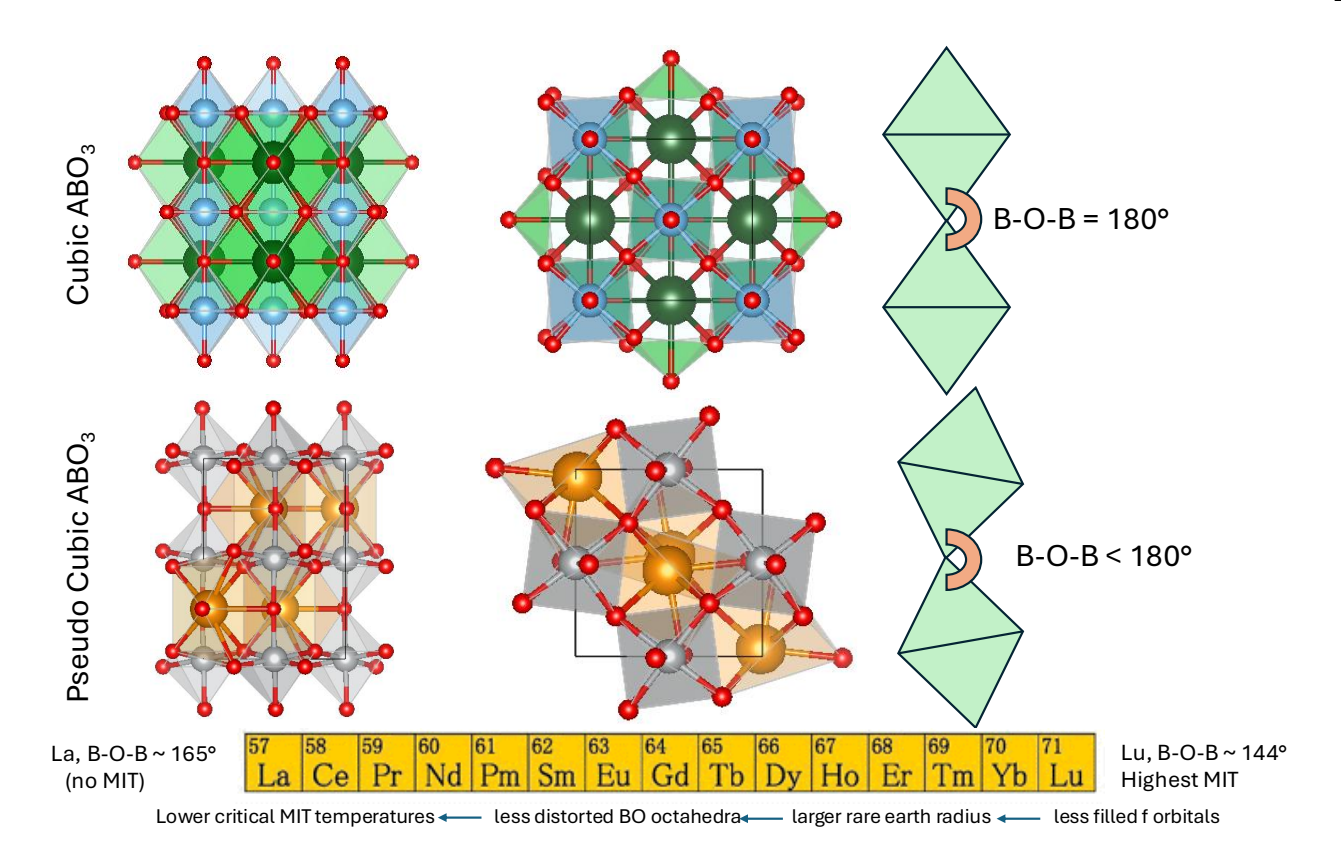


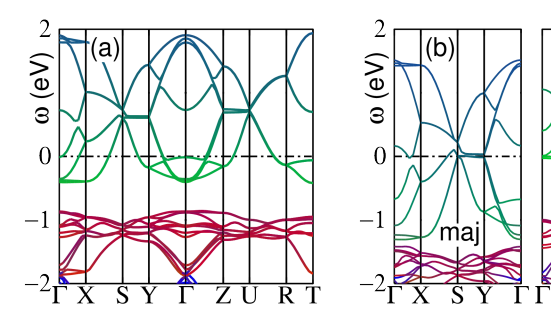
FIG. 1. Nature of the pseudo-cubic distortion in RNiO₃: In RNiO₃ compounds, the pseudo-cubic distortion causes the B-O-B bond angle (B is Ni in this case) to deviate from the ideal 180°. This distortion is influenced by the size of the rare-earth ion: ions with less-filled f-orbitals tend to have a larger ionic radius. As the rare-earth ionic radius increases, the degree of pseudo-cubic distortion decreases. Although there is a correlation between the metal-insulator transition (MIT) temperature and the extent of pseudo-cubic distortion, the orthorhombic Pbnm phase alone is not sufficient to support an insulating state. Achieving insulation requires an additional reduction in crystal symmetry beyond the Pbnm structure.

does magnetism play in enabling or stabilizing the structural distortion, and how does it influence the magnetic structure of the inequivalent Ni sites in the monoclinic phase?

This question echoes a broader debate often framed as a "chicken-and-egg" problem: is it the magnetism or the structural distortion that drives the MIT in systems where they occur at the same critical temperature? A classical example of this dilemma is found in VO_2 , where the rutile-to-monoclinic (M1) structural distortion is accompanied by a first-order MIT. Over the decades, extensive research has argued both for an electronically driven MIT via Mott mechanisms [10–17] and for a lattice-driven transition [18–24]. Recent advances in ultrafast spectroscopy have provided new tools to disentangle these coupled degrees of freedom. By probing systems on femtosecond timescales, it becomes possible to temporally separate the electronic and structural responses to external stimuli. In VO_2 , such studies have revealed that the electronic transition can precede the structural one, suggesting a decoupling of mechanisms that are otherwise entangled in equilibrium [17, 25, 26]. This approach offers a promising pathway to investigate similar questions in RNiO₃, where the coupling between spin, lattice, and charge degrees of freedom remains a central puzzle.

The theoretical investigation into this faces its own challenges: it is difficult to construct a theoretical framework that captures the interplay between structural distortions and magnetism across the entire phase diagram in an unbiased manner. This challenge is compounded by the limitations and ambiguities inherent in commonly used computational approaches such as DFT+U and dynamical mean-field theory (DMFT). DFT+U, while widely used, tends to favor magnetic solutions that can artificially open a gap in the electronic structure. This makes it difficult to disentangle whether the gap is a consequence of intrinsic magnetic ordering or an artifact of the method [27]. Moreover, the inclusion of inter-site Coulomb interactions (V) and Hund's coupling (J) introduces additional parameters that are often empirically chosen, further complicating interpretation [8].

On the other hand, DMFT provides a more sophisticated treatment of local electronic correlations and is particularly well-suited for capturing Mott physics and Kondo-like behavior. However, it suffers from its own set of challenges, including ambiguities in the choice of Hubbard parameters, double-counting corrections, and the embedding of the impurity problem into the lattice [28, 29]. Furthermore, conventional single-site DMFT is exact only in the limit of



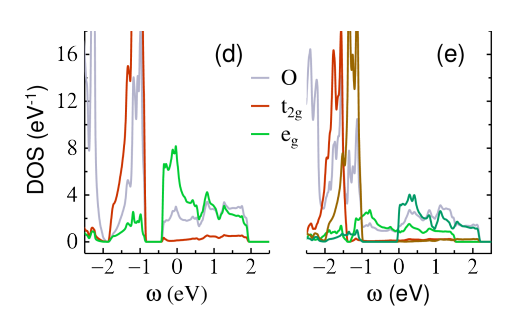


FIG. 2. NdNiO₃ in the pseudocubic Pbnm phase. (a) energy bands in the nonmagnetic case. The Γ-S-Y lines deviate from mirror images of the Γ-Z-U lines because of deviations from cubic symmetry. Colors represent the following projections: Ni- t_{2g} (red); Ni- e_g (green); O-p (blue); thus the e_g fall above the t_{2g} . (b,c) energy bands in the ferromagnetic case for (majority, minority) spins. The bands are similar except t_{2g} and e_g are spin split, enabling a gap to form in the minority channel. (d) Nonmagnetic density-of-states, showing the non-negligible amount of O character around E_F =0. (e) FM density-of-states, showing how the majority and minority Ni d states are spin split by ~1 eV. To distinguish spins, colors are modified to: t_{2g} (rust=majority, light-red=minority); e_g (green=majority, olive=minority); O-p (cornflower blue).

min

local interactions and fails to capture non-local correlations that are essential in systems like RNiO₃, where the MIT is accompanied by a symmetry-lowering distortion involving two inequivalent Ni sites. The nature of the monoclinic $P2_1/n$ distortion, which introduces Ni₁ and Ni₂ sublattices with distinct local environments, suggests that the minimal model capable of describing the insulating phase must include at least a two-site Ni cluster and their associated ligand states. This necessitates the use of cluster-DMFT approaches, which can capture inter-site correlations and the cooperative nature of the breathing-mode distortion [30]. While cluster DMFT is an attractive tool for NdNiO₃ and related compounds to explore the insulating nature of the low-temperature phase, [31] systematic disentangling of the causal relationship between structural symmetry breaking, magnetism, and the MIT remains a challenge within such framework.

To rigorously describe the electronic structure of the entire series from first principles, we employ a self-consistent implementation of many-body perturbation theory (MBPT) built into the Questaal package [32, 33]. A distinguishing feature of Questaal is its quasiparticle self-consistent form of GW, QSGW. GW is usually implemented as an extension to density-functional theory (DFT), i.e. G and W are generated from DFT. QSGW [34] may be thought of as an optimized form of the GW approximation of Hedin [35–37]. Self-consistency removes dependence on the starting point [35, 36] and also makes it possible to more systematically and reliably predict physical observables, especially those sensitive to self-consistency such as the magnetic moment [34] and response functions [38]. We address the MIT across the entire series by performing electronic structure calculations for seven candidate systems (R=Lu, Yb, Tm, Er, Ho, Nd, Pr). We find that the QSGW finds a metallic solution in the Pbnm phase and an insulating solution in the monoclinic phase, in agreement with experiments, for all candidate systems. Further, by artificially biasing a spin-disproportionate solution in the Pbnm phase and a spin-equivalent solution in the $P2_1/n$ phase we disentangle the role of structure and magnetism in driving the MIT. One key achievement of our work is that this disentanglement could be achieved without making any model Hamiltonian approximation and without any free parameters.

II. RESULTS

NON-MAGNETIC (NM) ELECTRONIC STRUCTURE IN Phnm PHASE

We begin by examining the electronic structure of NdNiO₃ in its high-symmetry Pbnm phase, as a representative example of the RNiO₃ family. NdNiO₃ is particularly interesting because it features both partially filled Ni-d and Nd-f states. However, the Nd-f orbitals lie well away the Fermi level (E_F) and do not contribute to the low-energy physics. Instead, the electronic structure near E_F is dominated by hybridized Ni-d and O-p states. In the Pbnm phase, all NiO₆ octahedra are crystallographically equivalent, and consequently, all Ni atoms exhibit identical spin and orbital moments. Our calculations reveal an unquenched orbital moment of approximately 0.10 μ_B per Ni atom. This is notably larger than the orbital moment observed in cubic NiO, which is about 0.03 μ_B [39]. The enhanced orbital moment in NdNiO₃ reflects the distinct electronic environment of Ni in RNiO₃ compared to NiO.

The key differences arise from both the nominal valence and the crystal field environment. In NiO, Ni is in a formal d^8 configuration, stabilized by a nearly perfect cubic crystal field that splits the d orbitals into a fully filled t_{2g}^6 and a half-filled e_g^2 manifold. This configuration supports strong electron-electron repulsion, leading to a Mott insulating

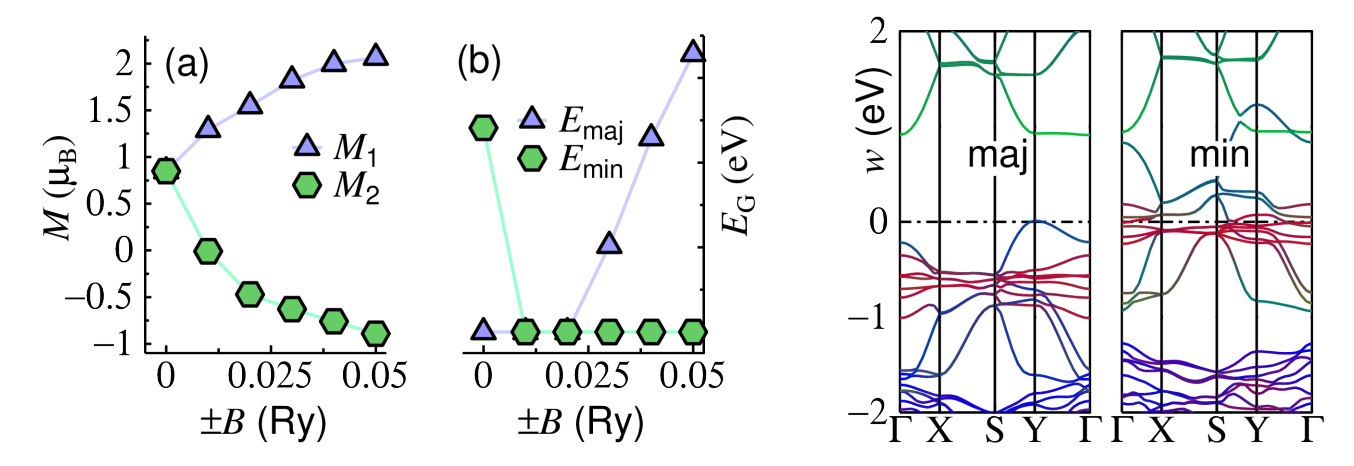


FIG. 3. Local magnetic moments (a) and bandgaps (b) of Pbnm NdNiO₃ in the presence of a site-local magnetic field $\pm B$. Right panels show energy bands for $B=0.04\,\mathrm{Ry}$.

state. In this case, the energy cost of double occupancy on a Ni site outweighs the kinetic energy gain from electron hopping, thereby localizing the electrons and opening a correlation-driven gap. Importantly, NiO remains insulating in both its magnetically ordered and disordered phases, underscoring the purely electronic nature of its insulating behavior. In contrast, Ni in RNiO₃ is nominally in a d^7 configuration, and the lower symmetry of the Pbnm phase introduces additional complexity through octahedral tilts and distortions. These structural features, combined with strong hybridization with oxygen, give rise to a more intricate interplay between lattice, spin, and orbital degrees of freedom, which is central to understanding the MIT in these materials.

CONSTRAINED SPIN-DISPROPORTIONATED ELECTRONIC STRUCTURE IN Phnm PHASE

To disentangle these mechanisms, we explore further different magnetic configurations of the Pbnm phase. A ferromagnetic solution of Pbnm can also be stabilized (Fig. 2(b,c)) with self-consistent moment 0.85 μ_B (all Ni sites are equivalent). The band structure is similar to the nonmagnetic one (Fig. 2(a)) except the Ni d states are spin split. As in the nm case states near E_F are predominantly of e_g character. Spin splitting enables a gap of $\sim 1 \, \mathrm{eV}$ to open in the minority channel, but not the majority. This offers the first hint that the MIT is driven by magnetism, and that the lattice distortion plays a secondary role. To open the gap, some form of antiferromagnetism is needed. To see this in more detail, consider adding a site-specific external Zeeman field B, driving the system ferrimagnetic. We do this by retaining only the mirror symmetry in z, which splits the four equivalent Ni into two inequivalent pairs. We apply B parallel or antiparallel to z on the respective equivalent sites, thus splitting moments into M_1 and M_2 , then carry the QS GW cycle to self-consistency for each B, and trace the evolution of M_1 , M_2 , and bandgaps with B. The result is shown in Fig. 3. Remarkably, the minority-spin gap closes with increasing B, while the majority-spin gap opens, with neither channel having a gap at intermediate B. As in the FM case, e_q falls above t_{2q} but a gap forms in a single channel only. (The matter is further complicated by the presence of states with O character.) This suggests that magnetism is the driving force for the MIT, but that Pbnm lacks sufficient configurational freedom to open the gap. For the monoclinic P2₁/n phase presented later, enough configurational freedom is available to open a gap in both channels, but in stark contrast to NiO where the spin configuration is of secondary importance, here the gap and local moments are closely connected. Thus the $P2_1/n$ distortion provides enough flexibility to enable a gap to open and reduce the orbital moment.

ANTIFERROMAGNETIC ELECTRONIC STRUCTURE IN P21/N PHASE

To further understand the insulating state in RNiO₃, we simulate the antiferromagnetic (AFM) phase in the low-symmetry monoclinic $P2_1/n$ structure. Capturing the experimentally observed AFM ordering vector $(\frac{1}{2},0,\frac{1}{2})$ requires doubling the Pbnm unit cell. This doubling naturally accommodates the breathing-mode distortion, which differentiates the NiO₆ octahedra into two distinct types: Ni₁ and Ni₂. Ni₁ resides in the larger octahedra with longer Ni–O bond lengths, while Ni₂ occupies the smaller octahedra with shorter bonds. The longer Ni–O bonds in Ni₁ reduce the hybridization between Ni-d and O-p states, enhancing electronic correlations and favoring a high-spin

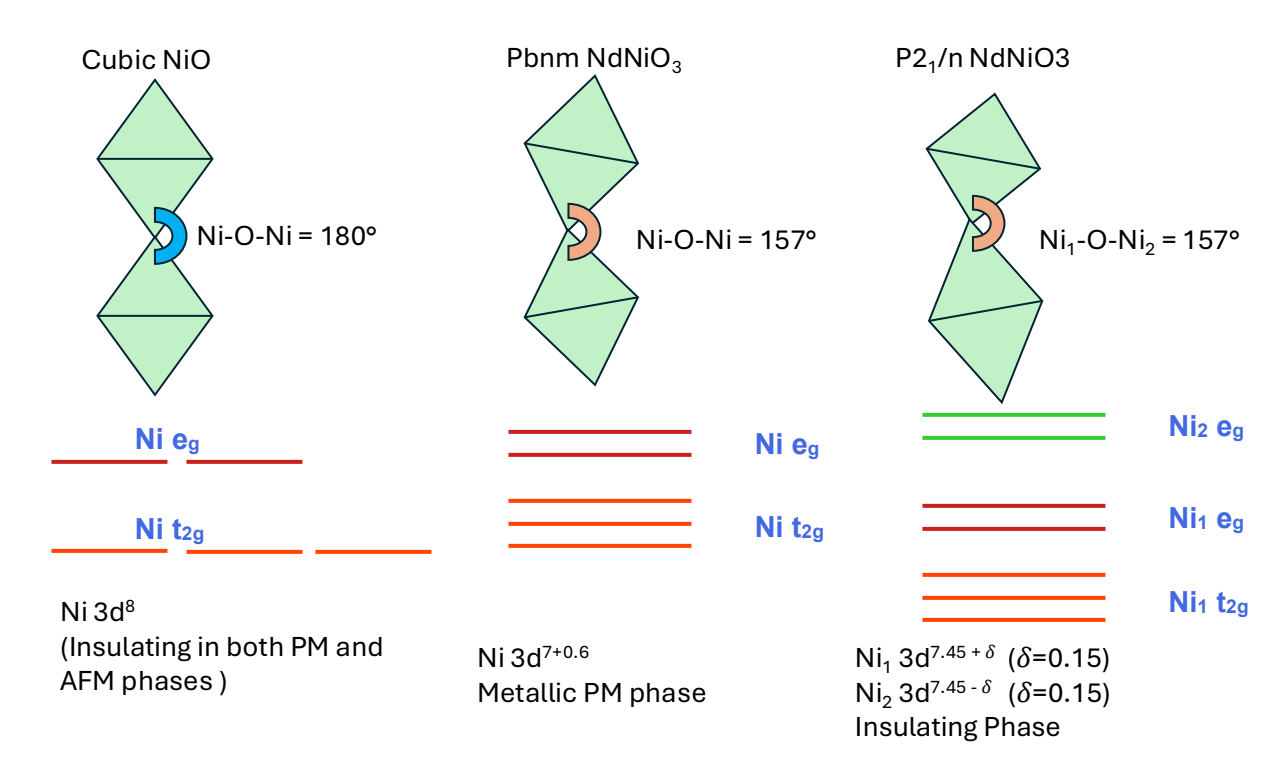


FIG. 4. Schematic representation of cubic, pseudo-cubic Pbnm and $P2_1/n$ distortions: NiO appears in cubic crystal field and is insulating in both the paramagnetic and antiferromagnetic phases. NdNiO₃ is a paramagnetic metal in the Pbnm phase and only becomes insulating in the $P2_1/n$ phase with a concomitant charge, spin and bond disproportionation. Note that the Ni-O-Ni bond angle does not change on average due to the Pbnm to $P2_1/n$ distortion. The corresponding crystal field diagrams are also shown for all cases. The insulating gap in $P2_1/n$ phase opens between the e_g states of the two distinct Ni sites, while in NiO the band gaps opens at a single Ni site.

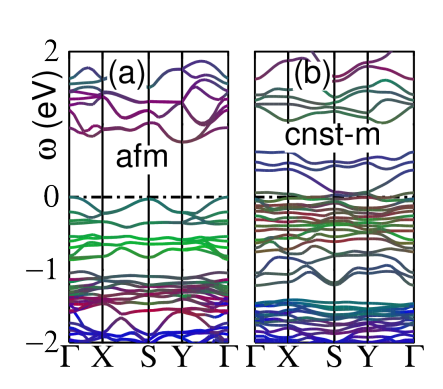
configuration. In contrast, Ni₂ experiences stronger ligand hybridization, stabilizing a low-spin state. This spinstate disproportionation is a hallmark of the insulating phase and is accompanied by charge and orbital moment disproportionation.

Our calculations show that the Nd-f states (and those of other rare-earth ions, except Y where unoccupied f states lie at $E_F + 6$ eV) lie far from the Fermi level, typically a few above and below, and do not contribute to the low-energy physics. All seven RNiO₃ compounds studied exhibit indirect band gaps in the AFM phase. For NdNiO₃, the valence band maximum (VBM) lies between E_F and $E_F - 0.5$ eV and is primarily composed of Ni₁ e_g orbitals ($m_l = -2, 0$), while the conduction band minimum (CBM) originates from the same orbitals on Ni₂. This orbital-selective gap is a clear signature of a magnetic gap opening between inequivalent Ni sites 4.

	$\langle Ni_1 - O \rangle - \langle Ni_2 - O \rangle$, Å	AFM gap in meV	AFM $\langle S \rangle$, Ni ₁ , Ni ₂ , μ_B
Y	0.071	700	1.21,0
Nd	0.071	750	1.225,0
Но	0.08	987	1.352,0
Er	0.08	821	1.294,0
Tm	0.094	988	1.358,0
Lu	0.084	905	1.34,0

TABLE I. Theoretically observed bond and spin disproportionation and their relation with computed band gaps across the series.

A significant quenching of the orbital moment is observed in the monoclinic phase compared to the high-symmetry Pbnm phase. Ni₁ retains an orbital moment of 0.074 μ_B and a spin moment of 1.3 μ_B , while Ni₂ exhibits complete quenching of both spin and orbital moments. This remarkable asymmetry is consistent across all RNiO₃ compounds studied, indicating that half of the Ni sites in the monoclinic phase become effectively non-magnetic (see Table I). The projected density of states reveals that Ni₁ t_{2g} states lie approximately 1 eV below E_F , while its e_g states form the



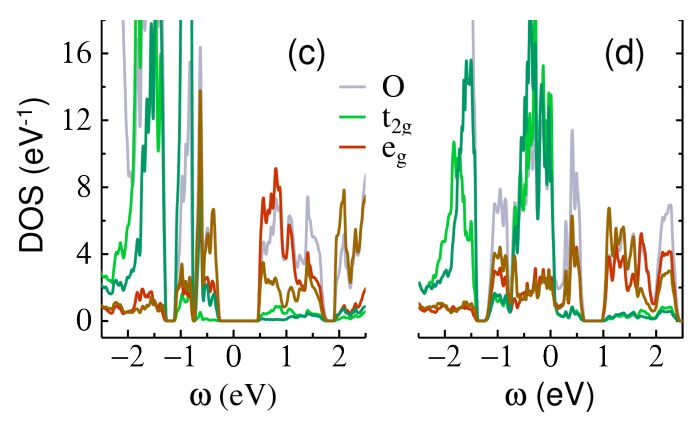


FIG. 5. **AFM** NdNiO₃ in P2₁/n phase: (a) Energy bands in AFM phase, and (b) the AFM phase with additional constraining fields as described in the text. (In both cases up- and down- bands are nearly equivalent.) Colors represent the following projections: Ni₁ (red); Ni₂ (green); O-p (blue). In the unconstrained case, Ni₁ and Ni₂ have local moments $\pm 1.22 \,\mu_B$ and 0, respectively. In the constrained case, Ni₁ and Ni₂ all have approximate moments $\pm 1.2 \,\mu_B$. (c,d) corresponding DOS. Colors represent the following projections: e_g (rust=Ni₁, bright-red=Ni₂); t_{2g} (olive=Ni₁, bright-green=Ni₂); O-p (cornflower blue).

top of the valence band. Conversely, $Ni_2 e_g$ states define the bottom of the conduction band. This band alignment is independent of whether FM, PM or AFM simulations are performed.

A Mulliken charge analysis reveals a real-space charge disproportionation: Ni₁ exhibits a $d^{7.6}$ configuration (4.5 electrons in the spin-up channel and 3.1 in spin-down), while Ni₂ has a $d^{7.3}$ configuration (3.55 electrons in each spin channel). This corresponds to a charge modulation of $d^{7.45\pm\delta}$ with $\delta\approx0.15$. Thus, the monoclinic distortion not only induces bond disproportionation but also drives charge, spin, and orbital moment disproportionation. This results in the spatial separation of two distinct Ni-d spin multiplets across the lattice. In the high-symmetry Pbnm phase, these multiplets are dynamically fluctuating and spatially equivalent, leading to a correlated metallic state. The structural distortion in the $P2_1/n$ phase breaks this symmetry, enabling the system to stabilize these multiplets in real space and open a robust insulating gap. Consequently, the band gap in the AFM insulating phase is fundamentally determined by the energy separation between the high-spin Ni₁ and low-spin Ni₂ e_q states.

CONSTRAINED SPIN-EQUIVALENT ELECTRONIC STRUCTURE IN P21/N PHASE

To show more explicitly that the MIT is a consequence of the bond-disproportionation achieved through unique combinations of Ni magnetic states, we perform a another calculation, now adding site-local Zeeman fields constraining all Ni moments to similar absolute values. Two kinds of fields are added, one on Ni₁ and another on Ni₂, to constrain the local moments on all Ni sites to be $\pm 1.2 \pm 0.2$ eV. (There is a small fluctuation in each moment owing to absence of symmetry.) The lattice is kept fixed at the breathing-mode distortion and the QSGW cycle is carried through to self-consistency. Energy band structures for the two cases are compared in Fig 5(a,b). Fig. 5(c,d) show the corresponding Mulliken DOS resolved into t_{2g} and e_g components for Ni₁ and Ni₂, and also O p character. Two key features stand out: First, that the occupied t_{2g} and e_g states split into two peaks, pushing states higher in energy; second that an Oderived state is split off from the conduction band and bonds with the Ni₁- e_g state, forming a "midgap" state around E_F . Thus the MIT is formed by a delicate interplay of several interlocking forces: stabilization through the formation of local spin moments (enabling a gap to open) while also quenching orbital moments through disproportionation; and also lattice distortions working in tandem with disproportionation to which sweep O p states away from the Fermi level.

III. DISCUSSION

The multi-determinantal nature of Mott physics remains a central and unresolved topic in the study of strongly correlated materials. When combined with structural instabilities, this becomes one of the outstanding problems in solid-state physics. From that point of view, NiO is relatively simple: it transitions from a paramagnetic insulating to an antiferromagnetic (AFM) insulating phase without undergoing structural changes. This simplicity makes it a valuable prototype for studying Mott physics. The classification of systems as truly Mott-like continues to generate

debate. NiO has long been considered a prototypical Mott insulator, often cited as a system that cannot be described within a conventional Slater framework, but originates from dynamical spin fluctuations. [40] Experimental and theoretical studies have shown that NiO exhibits a charge-transfer gap with strong local Coulomb interactions, consistent with the Zaanen-Sawatzky-Allen picture [41]. The Ni²⁺ ion in NiO adopts a d^8 configuration with a fully filled t_{2g} shell and two half-filled e_g orbitals, allowing for multiple atomic spin excitations ($\langle S \rangle = 1$ and $\langle S \rangle = 0$) on individual Ni sites. These dynamic spin fluctuations are hallmarks of Mott physics.

Our recent many-body perturbative studies [39], using a diagrammatic approach that incorporates long-range Coulomb interactions without frequency-dependent kernels, successfully reproduce the band gap of NiO. Moreover, the insulating state remains robust against changes in magnetic ordering, indicating that the gap is not solely tied to magnetic symmetry breaking. This challenges the traditional Mott narrative, yet the nature of the multi-particle excitations in NiO—such as spinful carriers introduced by weak hole doping and optical access to both singlet and triplet excitonic states supports its classification as a Mott system. These excitation spectra reflect the inherently multi-determinantal character of the Ni d-manifold, that can be reasonably captured within a single-site Hubbard model [40].

In contrast, RNiO₃ compounds exhibit multi-determinantal physics of a fundamentally different character. Here, the relevant determinants are spatially distributed across inequivalent Ni sites, making non-local correlations essential. The insulating state in RNiO₃ cannot be characterized in terms of a site-site, frequency-dependent description, but from real-space disproportionation of charge, spin, and orbital moments between Ni₁ and Ni₂ sites [42]. This spatial separation is stabilized by a monoclinic structural distortion that breaks the symmetry of the high-temperature metallic phase. A further distinction lies in the orbital moment behavior. In NiO, the d^8 configuration leads to a nearly quenched orbital moment due to high cubic symmetry and strong crystal field splitting. By contrast, Ni in RNiO₃ is in a d^7 configuration and exhibits a significantly larger unquenched orbital moment in the highsymmetry phase. Structural distortions such as Jahn-Teller [43, 44] or breathing-mode modulations [6] are known to lift orbital degeneracies and quench orbital moments in a range of systems, lowering the system's energy. Our theoretical framework shows that while disentangling these coupled degrees of freedom is challenging, the primary driving force behind the metal-insulator transition in RNiO₃ is magnetic in nature. The breathing-mode distortion plays a secondary, assisting role by enabling spatial separation of spin multiplets and quenching orbital moments. In summary, NiO exemplifies a Mott insulator governed by local interactions and dynamic fluctuations, whereas RNiO₃ represents a distinct class of correlated insulators where non-local interactions, structural symmetry breaking, and orbital moment quenching are intricately intertwined. The minimal Hamiltonian required to describe RNiO₃ must include at least two inequivalent Ni sites and their ligand environments, highlighting the need for theoretical frameworks that go beyond single-site approximations.

IV. METHODS: QUASIPARTICLE SELF-CONSISTENT GW

The Quasiparticle Self-Consistent GW form of GW [35, 36] dramatically improves its fidelity compared to the usual (DFT-based) GW. Details of the theory and its implementation in Questaal [33] can be found in Refs [32, 36]. QSGW largely eliminates the starting-point dependence (a well known issue for GW implementations) and importantly, discrepancies with experiment become systematic, which clarifies which diagrams are missing. Also, as a byproduct, QSGW yields the ground state magnetic structure, without reference to DFT-a feature particularly crucial in this study, where the magnetic ground state is the major question at issue. As this work shows, the fidelity achievable in QSGW and is essential to distinguish artifacts from lower level approximations.

DATA AVAILABILITY

All data will be available from the corresponding authors, SA, on reasonable request. All the input file structures and the command lines to launch calculations are rigorously explained in the tutorials available on the Questaal webpage [33] .

CODE AVAILABILITY

The source codes for LDA, QSGW and $QSG\widehat{W}$ are available from [33] under the terms of the AGPLv3 license.

- [1] F. Serrano-Sánchez, M. T. Fernández-Díaz, J. L. Martínez, and J. A. Alonso, "On the magnetic structure and magnetic behaviour of the most distorted member of the series of RNiO3 perovskites (R = Lu)," <u>Dalton Trans.</u>, vol. 51, pp. 2278–2286, 2022.
- [2] H. Guo, Z. Li, L. Zhao, Z. Hu, C. Chang, C.-Y. Kuo, W. Schmidt, A. Piovano, T. Pi, O. Sobolev, <u>et al.</u>, "Antiferromagnetic correlations in the metallic strongly correlated transition metal oxide lanio3," <u>Nature communications</u>, vol. 9, no. 1, p. 43, 2018.
- [3] M. Golalikhani, Q. Lei, R. U. Chandrasena, and et al, "Nature of the metal-insulator transition in few-unit-cell-thick LaNiO3 films," Nat Commun, vol. 9, p. 2206, 2018.
- [4] S. Catalano, M. Gibert, J. Fowlie, and et al., "Rare-earth nickelates RNiO3: thin films and heterostructures," Reports on Progress in Physics, vol. 81, no. 4, p. 046501, 2018.
- [5] A. Mercy, J. Bieder, J. Íñiguez, and P. Ghosez, "Structurally triggered metal-insulator transition in rare-earth nickelates," Nature Communications, vol. 8, no. 1, p. 1677, 2017.
- [6] D. I. Badrtdinov, A. Hampel, and C. E. Dreyer, "Interplay between breathing-mode distortions and magnetic order in rare-earth nickelates from ab initio magnetic models," Physical Review B, vol. 104, no. 5, p. 054403, 2021.
- [7] B. Lau and A. J. Millis, "Theory of the magnetic and metal-insulator transitions in RNiO3 bulk and layered structures," Physical Review Letters, vol. 110, no. 12, p. 126404, 2013.
- [8] L. Binci, M. Kotiuga, I. Timrov, and N. Marzari, "Hybridization driving distortions and multiferroicity in rare-earth nickelates," Physical Review Research, vol. 5, no. 3, p. 033146, 2023.
- [9] J. W. Freeland, M. van Veenendaal, and J. Chakhalian, "Evolution of Electronic Structure Across the Rare-Earth RNiO₃ Series," Journal of Electron Spectroscopy and Related Phenomena, 2015.
- [10] J. M. Tomczak, F. Aryasetiawan, and S. Biermann, "Effective bandstructure in the insulating phase versus strong dynamical correlations in metallic vo₂," Phys. Rev. B, vol. 78, p. 115103, Sep 2008.
- [11] R. Sakuma, T. Miyake, and F. Aryasetiawan, "Quasiparticle band structure of vanadium dioxide," <u>J. Phys.: Condens.</u> Matter, vol. 21, no. 6, p. 064226, 2009.
- [12] S. Biermann, A. Poteryaev, A. I. Lichtenstein, and A. Georges, "Dynamical singlets and correlation-assisted peierls transition in vo₂," Phys. Rev. Lett., vol. 94, p. 026404, Jan 2005.
- [13] W. H. Brito, M. C. O. Aguiar, K. Haule, and G. Kotliar, "Metal-insulator transition in vo₂: A DFT+DMFT perspective," Phys. Rev. Lett., vol. 117, p. 056402, Jul 2016.
- [14] O. Nájera, M. Civelli, V. Dobrosavljević, and M. J. Rozenberg, "Resolving the vo₂ controversy: Mott mechanism dominates the insulator-to-metal transition," Phys. Rev. B, vol. 95, p. 035113, Jan 2017.
- [15] J.-P. Pouget, "Basic aspects of the metal-insulator transition in vanadium dioxide VO₂: a critical review," <u>Comptes Rendus Physique</u>, vol. 22, no. 1, pp. 37–87, 2021.
- [16] $\overline{\text{C. Si, W. Xu, H.}}$ Wang, and et al., "Metal-insulator transition in $V_{1-x}W_xO_2$: structural and electronic origin," Physical Chemistry Chemical Physics, vol. 14, no. 43, pp. 14913–14919, 2012.
- [17] Y.-C. Lee, X. Guan, Q. Shi, and Y.-L. Huang, "Ultrafast Phase Transition in a VO₂ Membrane: The Role of Mechanics," ACS Applied Electronic Materials, 2023.
- [18] M. M. Qazilbash, A. A. Schafgans, K. S. Burch, S. J. Yun, B. G. Chae, B. J. Kim, H. T. Kim, and D. N. Basov, "Electrodynamics of the vanadium oxides Vo₂ and v₂o₃," Phys. Rev. B, vol. 77, p. 115121, Mar 2008.
- [19] J. H. Park, J. M. Coy, T. S. Kasirga, C. Huang, Z. Fei, S. Hunter, and D. H. Cobden, "Measurement of a solid-state triple point at the metal-insulator transition in vo2," Nature, vol. 500, pp. 431 EP –, 08 2013.
- [20] N. B. Aetukuri, A. X. Gray, M. Drouard, M. Cossale, L. Gao, A. H. Reid, R. Kukreja, H. Ohldag, C. A. Jenkins, E. Arenholz, K. P. Roche, H. A. Dürr, M. G. Samant, and S. S. P. Parkin, "Control of the metal-insulator transition in vanadium dioxide by modifying orbital occupancy," Nature Physics, vol. 9, pp. 661 EP -, 09 2013.
- [21] S. Cueff, D. Li, Y. Zhou, F. J. Wong, J. A. Kurvits, S. Ramanathan, and R. Zia, "Dynamic control of light emission faster than the lifetime limit using vo2 phase-change," Nature Communications, vol. 6, pp. 8636 EP –, 10 2015.
- [22] Z. Hiroi, "Structural instability of the rutile compounds and its relevance to the metal-insulator transition of vo2," Progress in Solid State Chemistry, vol. 43, no. 1-2, pp. 47–69, 2015.
- [23] J. del Valle, C. W. Rischau, A. Korshunov, D. Ambrosi, A. T. Martin-Luengo, I. Yousef, S. A. Lopez-Paz, S. Neyshtadt-Ronel, S. Gariglio, A. Bosak, et al., "A structural instability drives the vo2 metal-insulator transition," arXiv preprint arXiv:2501.15037, 2025.
- [24] C. Weber, S. Acharya, B. Cunningham, M. Grüning, L. Zhang, H. Zhao, Y. Tan, Y. Zhang, C. Zhang, K. Liu, et al., "Role of the lattice in the light-induced insulator-to-metal transition in vanadium dioxide," Physical Review Research, vol. 2, no. 2, p. 023076, 2020.
- [25] I.-H. Hwang, C.-I. Park, S. Yeo, C.-J. Sun, and S.-W. Han, "Decoupling the metal-insulator transition and crystal field effects of VO₂," <u>Scientific Reports</u>, vol. 11, p. 82588, 2021.
- [26] S. Han and et al., "Kinetically Decoupled Electrical and Structural Phase Transitions in VO₂," arXiv preprint, 2021.

- [27] E. Pavarini, E. Koch, R. Scalettar, and R. Martin, "Mott transition: DFT+U vs DFT+DMFT," in The Physics of Correlated Insulators, Metals, and Superconductors, Forschungszentrum Jülich, 2017.
- [28] H. Chen, A. Hampel, J. Karp, F. Lechermann, and A. J. Millis, "Dynamical Mean Field Studies of Infinite Layer Nickelates: Physics Results and Methodological Implications," Frontiers in Physics, vol. 10, p. 835942, 2022.
- [29] A. Carta, I. Timrov, A. Hampel, and C. Ederer, "Explicit demonstration of the equivalence between DFT+U and the Hartree-Fock limit of DFT+DMFT," Physical Review Research, vol. 7, no. 1, p. 013289, 2025.
- [30] K. Fursich, Y. Lu, D. Betto, and et al., "Resonant inelastic x-ray scattering study of bond order and spin excitations in nickelate thin-film structures," arXiv preprint.
- [31] J. Li, J. Pelliciari, C. Mazzoli, and et al., "Scale-invariant magnetic textures in the strongly correlated oxide NdNiO₃," Nature Communications, vol. 10, p. 4561, 2019.
- [32] D. Pashov, S. Acharya, W. R. L. Lambrecht, J. Jackson, K. D. Belashchenko, A. Chantis, F. Jamet, and M. van Schilfgaarde, "Questaal: a package of electronic structure methods based on the linear muffin-tin orbital technique," Comp. Phys. Comm., vol. 249, p. 107065, 2020.
- [33] https://www.questaal.org. Questaal code website.
- [34] S. V. Faleev, M. van Schilfgaarde, and T. Kotani, "All-electron self-consistent GW approximation: Application to Si, MnO, and NiO," Phys. Rev. Lett, vol. 93, p. 126406, 2004.
- [35] M. van Schilfgaarde, T. Kotani, and S. Faleev, "Quasiparticle Self-Consistent GW Theory," Phys. Rev. Lett., vol. 96, no. 22, p. 226402, 2006.
- [36] T. Kotani, M. van Schilfgaarde, and S. V. Faleev, "Quasiparticle self-consistent <u>GW</u> method: A basis for the independent-particle approximation," PRB, vol. 76, p. 165106, 2007.
- [37] S. Ismail-Beigi, "Justifying quasiparticle self-consistent schemes via gradient optimization in Baym–Kadanoff theory," <u>J.</u> Phys.: Condens. Matter, vol. 29, p. 385501, 2017.
- [38] S. Acharya, D. Pashov, A. N. Rudenko, M. Rösner, M. van Schilfgaarde, and M. I. Katsnelson, "Importance of charge self-consistency in first-principles description of strongly correlated systems," npj Comput. Mater, vol. 7, p. 208, 2021.
- [39] S. Acharya, D. Pashov, C. Weber, M. van Schilfgaarde, A. I. Lichtenstein, and M. I. Katsnelson, "A theory for colors of strongly correlated electronic systems," Nature Communications, vol. 14, no. 1, p. 5565, 2023.
- [40] X. Ren, I. Leonov, G. Keller, M. Kollar, I. Nekrasov, and D. Vollhardt, "LDA + DMFT computation of the electronic spectrum of NiO," Phys. Rev. B, vol. 74, p. 195114, Nov 2006.
- [41] F. Wrobel, H. Park, C. Sohn, H.-W. Hsiao, J.-M. Zuo, H. Shin, H. N. Lee, P. Ganesh, and A. Benali, "Doped NiO: The mottness of a charge transfer insulator," Physical Review B, vol. 101, no. 19, p. 195128, 2020.
- [42] Y. Cui, X. Liu, W. Fan, J. Ren, and Y. Gao, "Metal-insulator transition in RNiO₃ (R = Pr, Nd, Sm, Gd, Tb, Dy, Ho, Er) induced by Li doping: A first-principles study," Journal of Applied Physics, vol. 129, no. 23, p. 235107, 2021.
- [43] M. A. Halcrow, "Jahn-Teller distortions in transition metal compounds, and their importance in functional molecular and inorganic materials," Chemical Society Reviews, vol. 42, no. 4, pp. 1784–1795, 2013.
- [44] T. Shang, A. Gao, D. Xiao, Q. Zhang, X. Rong, Z. Tang, W. Lin, T. Lin, F. Meng, and X. Li, "An orbital strategy for regulating the Jahn–Teller effect," National Science Review, vol. 11, no. 9, p. nwae255, 2024.

ACKNOWLEDGMENTS

This work was authored in part by the National Renewable Energy Laboratory for the U.S. Department of Energy (DOE) under Contract No. DE-AC36-08GO28308. Funding was provided by the Office of Science, Basic Energy Sciences, Division of Materials, U.S. Department of Energy. SA, DP and MvS acknowledge the use of the National Energy Research Scientific Computing Center, under Contract No. DE-AC02-05CH11231 using NERSC award BES-ERCAP0021783, and also acknowledge that a portion of the research was performed using computational resources sponsored by the Department of Energy's Office of Energy Efficiency and Renewable Energy and located at the National Renewable Energy Laboratory, and computational resources provided by the Oakridge leadership Computing Facility. The views expressed in the article do not necessarily represent the views of the DOE or the U.S. Government. The U.S. Government retains and the publisher, by accepting the article for publication, acknowledges that the U.S. Government retains a nonexclusive, paid-up, irrevocable, worldwide license to publish or reproduce the published form of this work, or allow others to do so, for U.S. Government purposes.

AUTHOR CONTRIBUTIONS

SA conceived the work and carried out the calculations and drafted the paper. MvS and DP provided the necessary software and calculation support. BT, KA and JB provided experimental insights. All authors have contributed to the writing of the paper and the analysis of the data.

COMPETING INTERESTS

The authors declare no competing financial or non-financial interests.

CORRESPONDENCE

All correspondence and additional code and data requests should be made to SA.